FFI RAPPORT

SUMMARY REPORT ON ANALYSIS OF ACOUSTIC DATA FROM THE SWASI-99 ARRAY EXPERIMENT

EIDEM Ellen Johanne, JENSERUD Trond,
SØSTRAND Knut, TOLLEFSEN Dag

FFI/RAPPORT-2003/01374

FFIBM/786/044

Approved
Horten 15. December 2003

Jarl K Johnsen
Director of Research

SUMMARY REPORT ON ANALYSIS OF ACOUSTIC DATA FROM THE SWASI-99 ARRAY EXPERIMENT

EIDEM Ellen Johanne, JENSERUD Trond,
SØSTRAND Knut, TOLLEFSEN Dag

FFI/RAPPORT-2003/01374

FORSVARETS FORSKNINGSINSTITUTT
Norwegian Defence Research Establishment
P O Box 25, NO-2027 Kjeller, Norway

FORSVARETS FORSKNINGSINSTITUTT (FFI)
Norwegian Defence Research Establishment

P O BOX 25
N0-2027 KJELLER, NORWAY

UNCLASSIFIED

SECURITY CLASSIFICATION OF THIS PAGE (when data entered)

REPORT DOCUMENTATION PAGE

1) PUBL/REPORT NUMBER	2) SECURITY CLASSIFICATION	3) NUMBER OF PAGES
FFI/RAPPORT-2003/01374	UNCLASSIFIED	38
1a) PROJECT REFERENCE	**2a) DECLASSIFICATION/DOWNGRADING SCHEDULE**	
FFIBM/786/044	-	

4) TITLE

SUMMARY REPORT ON ANALYSIS OF ACOUSTIC DATA FROM THE SWASI-99 ARRAY EXPERIMENT

5) NAMES OF AUTHOR(S) IN FULL (surname first)

EIDEM Ellen Johanne, JENSERUD Trond, SØSTRAND Knut, TOLLEFSEN Dag

6) DISTRIBUTION STATEMENT

Approved for public release. Distribution unlimited. (Offentlig tilgjengelig)

7) INDEXING TERMS

IN ENGLISH:	IN NORWEGIAN:
a) Source localization	a) Posisjonsbestemmelse
b) Matched-field processing	b) Medietilpasset signalbehandling
c) Geoacoustic inversion	c) Geoakustisk inversjon
d) Vertical array	d) Antenner - vertikale
e) Horizontal array	e) Antenner - horisontale

THESAURUS REFERENCE:

8) ABSTRACT

The localization of underwater acoustic sources in a shallow water environment is addressed. Two array signal processing methods suitable for low-frequency signals in shallow water have been applied to data from an experiment conducted in the Barents Sea in 1999. The first method (matched-field processing) incorporates a full-field model of the acoustic signal in the signal processor. This method has been applied to vertical array data and to endfire horizontal array data. The second method (β-method) utilizes waveguide characteristics of the acoustic signal as measured on an endfire array and knowledge of the bathymetry of the propagation channel. A localization technique using data from a single hydrophone is also presented.

9) DATE	AUTHORIZED BY	POSITION
	This page only	
15. December 2003	Jarl K Johnsen	Director of Research

ISBN-82-464-0786-4

UNCLASSIFIED

SECURITY CLASSIFICATION OF THIS PAGE (when data entered)

CONTENTS

SUMMARY REPORT ON ANALYSIS OF ACOUSTIC DATA FROM THE SWASI-99 ARRAY EXPERIMENT

1 INTRODUCTION

The localization of acoustic sources can be a difficult problem in shallow water. Acoustic signals will here interact with the sea surface and seabed and acquire characteristics of waveguide propagation. The signals can then in general not be adequately analyzed using a conventional plane-wave description. Several alternative signal processing methods that extract and exploit these characteristics have been devised. One such method, matched-field processing (MFP) (1)(2), incorporates a model of the acoustic propagation into the signal processor. This method has been subject to research and applied with good results in several shallow water regions over the last decade (3)(4). The potential success of MFP is dependent on an accurate description of the propagation environment, specifically of the seabed. Parallel to the development of MFP as a technique for source localization, it has been developed as a method for the estimation of seabed parameters from measured acoustic fields. Matched-field inversion techniques have shown considerable promise (5) and offer a good alternative to the often more costly methods of in-situ collection of seabed data.

To test matched-field and other signal processing methods in a shallow water area, an experiment was conducted by Forsvarets forskningsinstitutt (FFI) in the Barents Sea in August 1999 (6). The experiment made use of broadband explosive sources and a receiving acoustic array deployed with a vertical section and a bottom-laid horizontal section. Results from processing of data from this experiment have been documented in a sequence of technical reports and conference proceedings. The present report summarizes the research conducted and the results obtained.

This report is organized as follows. Details of the Barents Sea experiment are outlined in Chapter 2. Chapter 3 outlines and discusses results obtained by matched-field processing of data from the vertical array. Chapter 4 treats results obtained by processing of data from the horizontal array. Some characteristics of the acoustic signals are exemplified and discussed in Chapter 5. In Chapter 6, a special technique for estimating source range using a property of the waveguide and data from the horizontal array is outlined. Chapter 7 discusses a technique for localization using data from a single hydrophone. A brief summary is found in Chapter 8.

2 THE SWASI-99 EXPERIMENT

by Ellen Johanne Eidem

The SWASI-99 experiment took place in the Barents Sea 2 – 8 August 1999 (6)(7). The area is relatively flat and far from the coast. The antenna was deployed in an upright L-shape at approximately 320 m water depth as illustrated in Figure 2.1. The vertical part of the antenna consisted of 21 hydrophones with spacing 10 m. The horizontal part consisted of 10 hydrophones with spacing from 20 m through 240 m as shown in Figure 2.2. The hydrophones had pre-amplifier 12 dB or 32 dB. The sampling frequency was 3051.8 Hz, and the data was recorded in time tagged sequences of 506 samples. Each sequence lasted 0.1658 s. Detailed description of the array configuration and acquisition system are found in (8)(9). The tilt of the vertical array was monitored continuously at three depth positions. The receiver station was onboard FFI's research vessel R/V H U SVERDRUP II, which also deployed and retrieved the antenna.

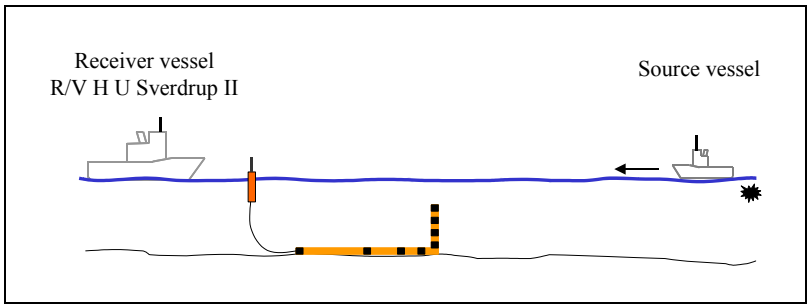

Figure 2.1 *Illustration of the SWASI-99 experiment. The source vessel dropped SUS charges at constant intervals. The array was deployed in an upright L-shape at about 320 m water depth.*

The source vessel sailed three run lines deploying small explosive charges at constant intervals. Two of the runs were endfire to the horizontal array, while the third was broadside. The run lengths were 116 km, 114 km and 66 km. The run lines are shown in the left panel in Figure 2.3. Flow noise due to the tidal current dominated the signals received at the vertical array below 30-40 Hz. When the tidal current was at strongest, the experiment was stopped preliminary. Detonation times and source signals were recorded onboard the source vessel using a towed hydrophone. The nominal detonation depths alternated between 18 m, 91 m and 244 m, while the actual detonation depths were found from the measured bubble pulse periods. During the three runs 355 charges were deployed. Figure 2.4 shows the time series of a shallow shot at range 37 km.

The position of the source vessel was recorded using a p-code GPS, while the position of the antenna was estimated using calibration shots and nearby shots (10). The horizontal range between the source and the vertical array was estimated using positioning and geometric information. The right panel in Figure 2.3 shows the sound speed profiles at the source

positions measured directly using XSV's or computed from the XCTD's or XBT's. The profiles are plotted on top of each other. There was a warmer surface layer of thickness 20-40 m with sound velocity 1482-1490 m/s, and a colder bottom layer with sound velocity down to 1463 m/s. The average sound velocity for the five XCTD's was 1473 m/s.

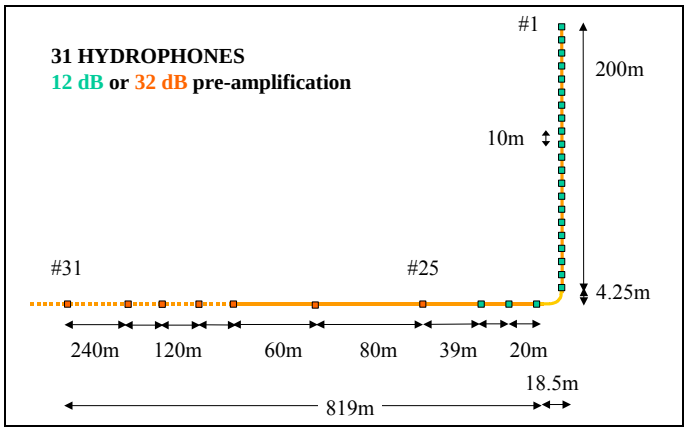

Figure 2.2 *The configuration of the array. Acoustic data was collected from 31 hydrophones. The bearing of the horizontal array was 295.7°.*

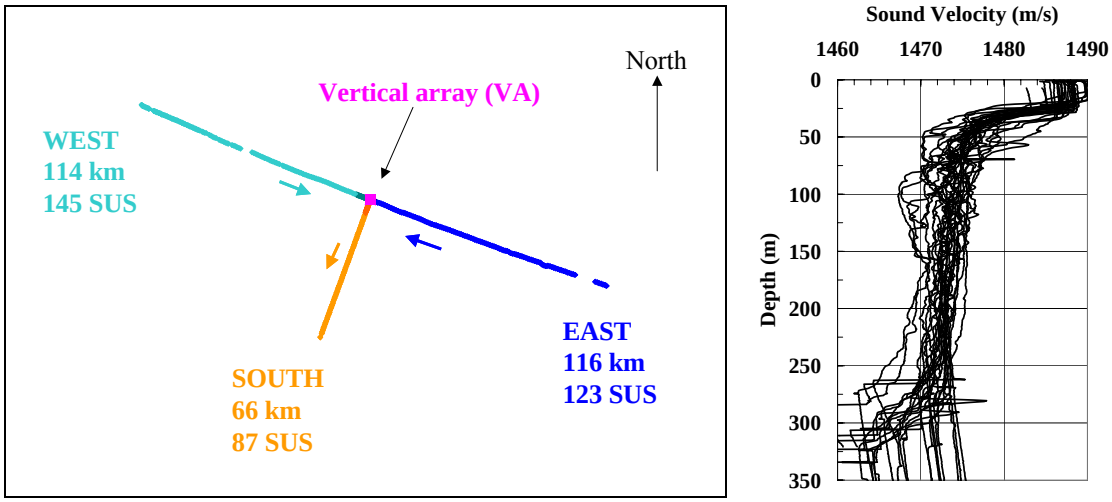

Figure 2.3 *Left: The three run lines in the SWASI-99 experiment. In total 355 SUS charges were deployed. The position of the vertical array is indicated. The arrows indicate the heading of the source vessel. Right: The sound speed profiles at the source positions plotted on top of each other. The profiles were either measured directly using XSV's or computed from XCTD's/XBT's.*

Seismic reflection and refraction measurements were carried out a few days after the acoustic experiment (11). The data showed a weakly range-dependent two-layer bottom with a sediment layer above a semi-infinite bedrock or substrate, see Figure 2.5. The water depth varied between 260 m and 360 m. From the literature the sediment layer is assumed to have a sound velocity of about 1800 m/s, with a density of 2.0 g/cm^3 (12). The sediment thickness varied between 10 m and 100 m, with 37 m at the receiver position. The bedrock consisted of mudstone, and close to the vertical array the sound velocity was measured to be about 2400 m/s. The density in the substrate was estimated from the sound velocity to be 2.2 g/cm^3.

At the west end of the western run salt domes were observed. From the literature these have a sound speed of about 5500 m/s (13).

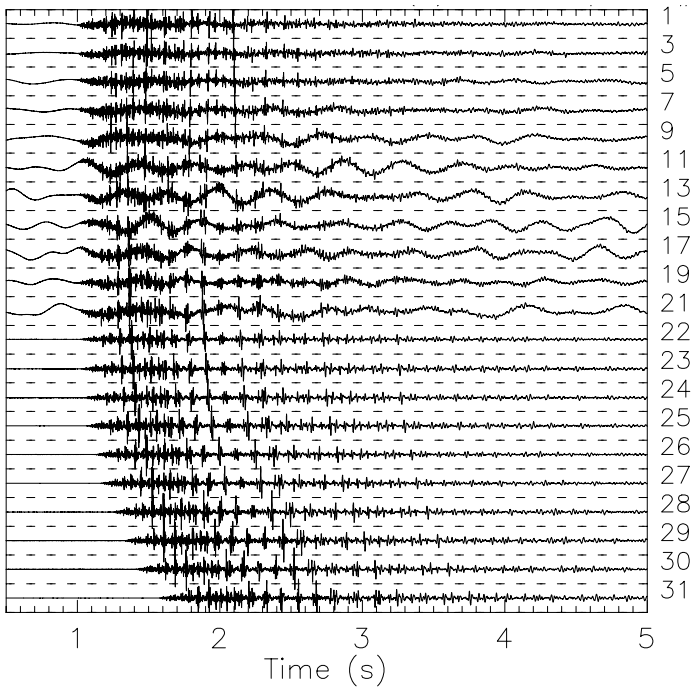

Figure 2.4 *The time series of an 18 m shot at range 37 km east. The hydrophone numbers are listed to the right. The low-frequency flow noise is easily observed at the vertical hydrophones.*

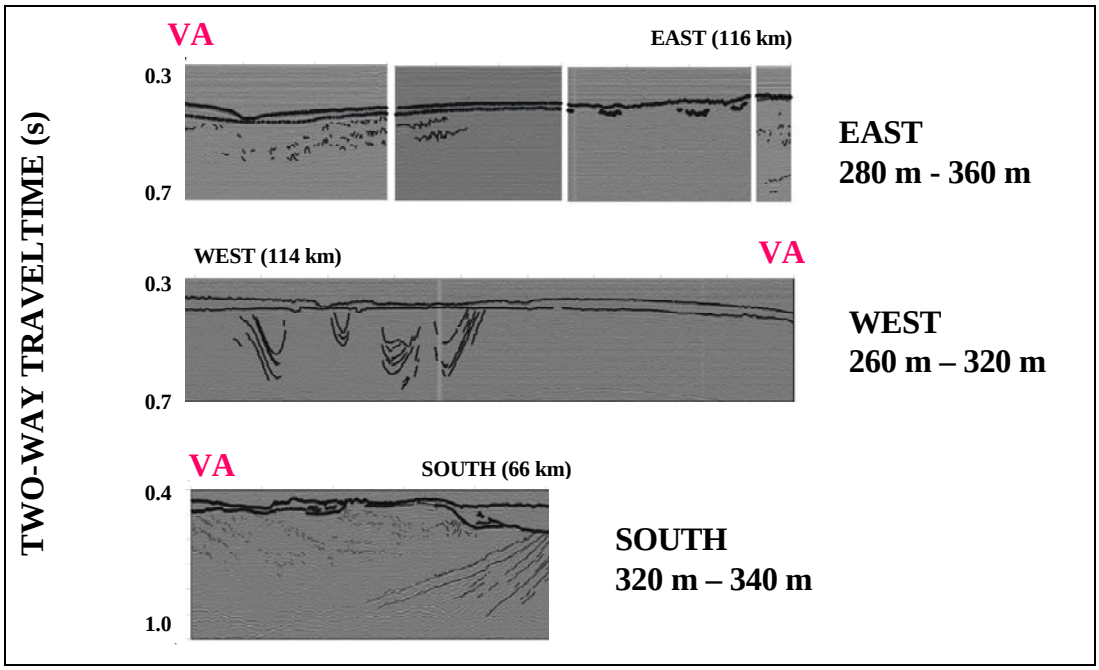

Figure 2.5 *The seismic profiles for the three run lines in SWASI-99 experiment. The water depth varied between 260 m and 360 m. The position of the vertical array (VA) is indicated. The bottom consisted of a sediment layer above the bedrock or substrate. In the western run salt domes were observed at the west end.*

3 INVERSION AND LOCALIZATION OF SHOTS BY MATCHED FIELDS USING A VERTICAL ARRAY

by Ellen Johanne Eidem

3.1 Background

Inversion and localization by matched-field processing techniques using the vertical array data from the SWASI-99 experiment have been reported in (14)(15)(16). In (14) a single shot was processed at single frequencies or by averaging over up to three frequencies. In (15) seven nearby shots were processed and inversion was carried out at both single frequencies and by averaging over 15 frequencies with high signal-to-noise ratio. In (16) source localization was carried out for more than 300 shots by averaging over 15 frequencies, independently of the signal-to-noise ratio. In this chapter the results from mainly (16) are presented.

3.2 Processing

The matched-field processing is carried out using the inversion tool SAGA (17), while the normal mode model C-SNAP is used to compute the synthetic field for a range-independent environment (18). The normalized Bartlett processor Φ is selected for the objective function

$$\Phi = \frac{1}{N_{freq}} \sum_{k=1}^{N_{freq}} \frac{\mathbf{q}^{\dagger}(\mathbf{m},\omega_k)\mathbf{R}(\omega_k)\mathbf{q}(\mathbf{m},\omega_k)}{\|\mathbf{q}\|^2 \|\mathbf{p}\|^2} \tag{3.1}$$

where **m** is the model vector, the covariance matrix **R** is the non-averaged outer product of the measured, complex pressure vector **p**, and **q** is the normalized simulated pressure vector at selected frequencies ω_k. The summation is over equally weighted frequencies. The Bartlett energy is in this chapter defined as $E = 1 - \Phi$. With perfect match between the simulated and measured data the Bartlett energy is zero. For minimizing the objective function, genetic algorithms are used. The best of all estimate associated with the best fit or lowest energy of the objective function is extracted and reported. The number of forward computations, population size and parallel populations are 3000, 64 and 40 respectively, if nothing else is noted. The crossover rate, reproduction size and mutation rate are as recommended in (17).

As input data to the processing, the covariance matrix is computed at 15 frequencies using a rectangular window and an FFT size of 40 sequences (covering in total 6.6 s and starting about 1 s before the first pulse arrival). The frequencies are grouped in three bands, each band covering 3 Hz. The centre frequencies are if nothing else noted: 41.0 Hz, 48.6 Hz and 56.4 Hz. Based on a priori information from the oceanographic and seismic measurements, a range-independent model consisting of semi-infinite vacuum, one sediment layer and a semi-infinite substrate layer is set up as shown in Figure 3.1. The water column is divided into five

water layers (three iso-velocity and two gradient layers of thickness 1 m) if nothing else is noted. The water depth is set to 319 m. The sediment thickness is 37 m, while the sediment velocity is 1800 m/s. The two-way travel time through the sediment is then as measured from the seismic data at the receiver position. No shear effects are assumed.

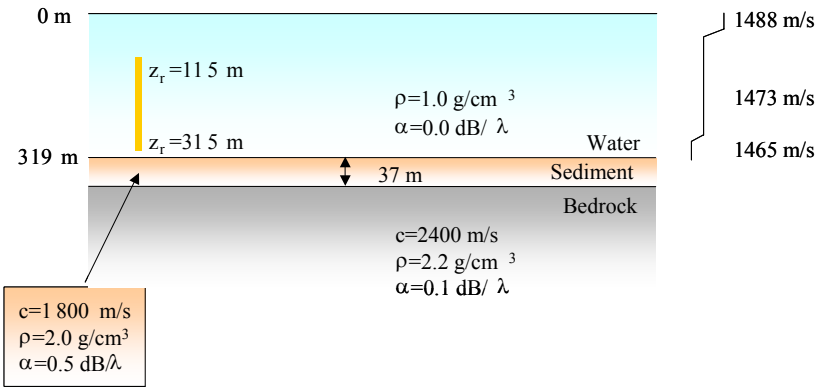

Figure 3.1 The environmental model used as input to SAGA.

3.3 Results

3.3.1 Sensitivity studies and ambiguity surfaces

Sensitivity analysis is carried out in order to determine which geoacoustic and geometric parameters are the most sensitive at the 15 frequencies selected, with a vertical receiver as used in the experiment. The Bartlett energy E is computed changing only one parameter at a time, while the remaining parameters are kept at their baseline values. The sensitivities of ten parameters are shown in Figure 3.2 for a synthetic shot at range 10 km. The most sensitive parameter is the water depth, followed by the top sediment velocity. For both parameters the sensitivity increases with range. The bottom sediment velocity is not a very sensitive parameter. A mismatch in the sediment thickness is of importance if the layer is thinner than assumed. The sensitivity of the sediment attenuation is low at 10 km, but increasing somewhat at 100 km (not shown here). The three substrate parameters velocity, density and attenuation are for practical purposes not sensitive at long ranges. The sensitivity of the first receiver depth (translation of entire array) is also low, especially at 100 km. The mismatch needs to be of several meters to be of importance, which is interesting to note since the sensitivity of the water depth is much higher. The largest change in parameter sensitivity going from short to long range is observed for the sediment density. At 10 km this is not a very sensitive parameter. However at 100 km the sensitivity has changed dramatically. A correlation plot between the sediment density and velocity shows that these two parameters are strongly correlated at 100 km, but not at 10 km.

Ambiguity surfaces will show the Bartlett energy at each allowable position of range and source depth. In (16) ambiguity surfaces of synthetic data are discussed in detail. To summarize, at 10 km range the source is well estimated in range and depth for all three source depths. Going to 100 km range a shallow source is also well estimated in depth and range,

while the two deeper sources have in addition sidelobes at other ranges and other depths complicating the localization.

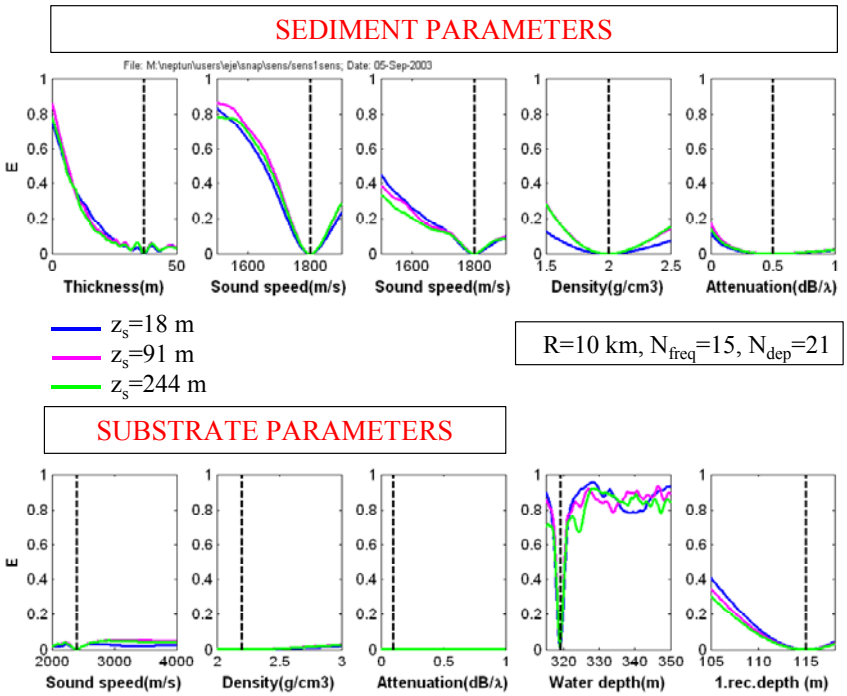

Figure 3.2 *Sensitivity study of the ten parameters sediment thickness, top and bottom sediment velocity, sediment density and attenuation, substrate velocity, density and attenuation, water depth and first receiver depth (i e translation of the entire array). Range 10 km. Three source depths. Vertical array of 21 elements with 10 m spacing. Fifteen frequencies between 39-59 Hz.*

3.3.2 Inversion of environmental parameters

Seven nearby shots (range 3-9 km) in the eastern run are inverted using 15 frequencies spread out in three bands with each band covering 3 Hz. The centre frequencies vary from 41.0-94.4 Hz. The baseline model is as presented earlier, but without the gradient water layers. Hence the water column is divided in three iso-velocity layers. The number of forward computations, population size and number of parallel populations are 3000, 64 and 6 respectively. Inversion of the six parameters water depth, sediment thickness, top sediment velocity, substrate velocity, sediment density and sediment attenuation is carried out five times for each of the seven shots. Figure 3.3 shows the 35 estimates for sediment and substrate velocity. The top sediment velocity is estimated to be 1612±45 m/s, which is about 200 m/s lower than in the baseline model. The reduction indicates that only the upper part of the seafloor is illuminated at these short ranges, while the value found from the seismic measurements and used in the baseline model represents the average sediment velocity throughout the entire layer. The substrate velocity is estimated to be 2396±443 m/s. The standard deviation is very high, however consistent with a low sensitivity for this parameter as predicted in the sensitivity studies. The sediment thickness estimate is 37±7 m, while the estimate for the sediment density is 2.1±0.2 g/cm^3. Hence the baseline values are within the

standard deviations. The sediment attenuation is estimated to be 0.18±0.10 dB/λ, which is lower than the baseline value of 0.5 dB/λ. The relatively large standard deviation indicates however less sensitivity for this parameter.

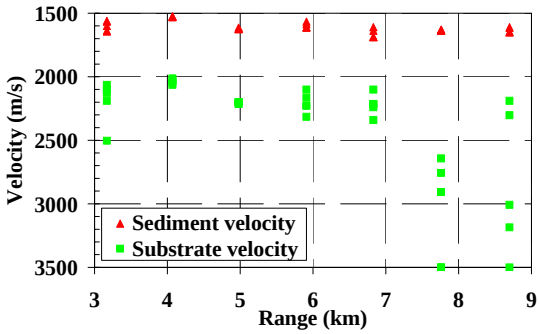

Figure 3.3 *Estimates for top sediment velocity and substrate velocity inverting shots in the eastern run at 3-9 km range. Five estimates per shot/parameter.*

3.3.3 Source localization

Source localization is carried out for more than 300 shots (19). The left panel of Figure 3.4 shows the range estimates for the eastern run inverting the six parameters: water depth, array tilt, sediment density and sediment velocity, in addition to source-receiver range and source depth. The largest variations in the range estimates are observed during periods dominated by flow noise due to the tidal current. A threshold for the Bartlett energy is introduced in order to remove the noisy periods and other range estimates with poor match. The value of the threshold is chosen by inspection of the data. Range estimates for all shots with Bartlett energy E<0.68 are shown in the right panel of Figure 3.4. Of the shots with Bartlett energy less than the threshold, 97% are within ± 15% of true range and 63% are within ±10% of true range. Similar results are found for the southern run, however for the western run the range estimates are not so good. This may be explained by a combination of flow noise and bathymetry. The localizations are successful out to 40 km, and possibly the salt domes complicates the geoacoustics at longer ranges, in addition to the tidal current.

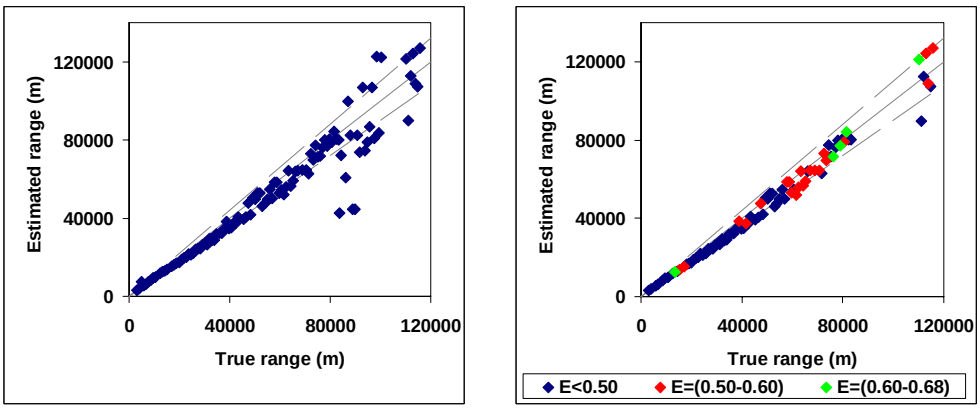

Figure 3.4 *Range estimates for all shots in the eastern run and for shots with Bartlett energy E<0.68. 6-parameter inversion.*

Going back to the eastern run, Figure 3.5 shows the relative error in the range estimates plotted versus true range. For the shallow sources the range errors seem to be systematic from shot to shot and following the bathymetric profile, indicating that the range estimates are biased. The sources are underestimated in range when the water depth is increasing and overestimated when the water depth is decreasing, as seen from the receiver position. Clearly, the shallow sources are easier to localize correct in range than the deeper sources, a result in agreement with the simulation studies. When thinning the array from 21 elements to five elements or shortening the aperture from 200 m to 90 m, the range estimates degrade, however not dramatically.

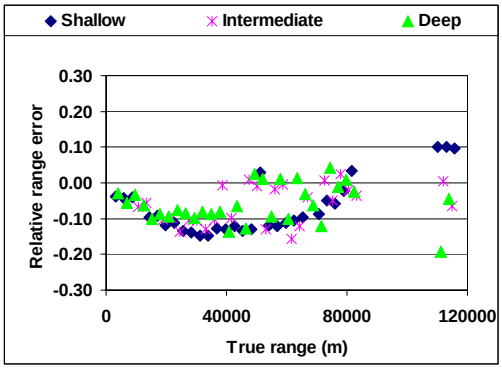

Figure 3.5 *Relative error in range estimates for all the shots in the eastern run with Bartlett energy E<0.68.*

The left panel of Figure 3.6 shows the source depth estimates for all the shots in the eastern run with Bartlett energy E<0.68. Also shown is the true source depth computed from the measured bubble pulse period. The shallow 18 m shots are well estimated in depth, while the estimates break down for the intermediate 91 m and deep 244 m shots at ranges beyond 40-50 km. Similar good results are obtained for the western and southern run regarding the shallow sources, however the source depth estimates for deeper sources are not as good as for the eastern run. Estimates for the water depth are shown in the right panel of Figure 3.6. The lower search bound is restricted due to the fixed array. The upper search bound is 350 m. For comparison an effective water depth $D_{EFF}=\sqrt{D_r \cdot D_s(r)}$ is computed, where D_r and D_s are the water depth at the receiver and source position, respectively and r is the range. For the eastern run the water depth estimates for the shallow shots show a depression close to the array in accordance with the depression in the effective water depth, however not to the same extent. The estimates vary only slightly from shot to shot. The water depth estimates for the deeper shots vary more.

Figure 3.7 shows the estimates for top sediment velocity and sediment density. The Y-axes span the search interval. The top sediment velocity is 1589±82 m/s, which is in agreement with the inversion results at 3-9 km range. The sediment density is 2.01±0.22 g/cm^3. For both parameters a trend line is plotted, showing increasing estimates with range. The large variation in the estimates indicates that the long-range shots are less sensitive to the two sediment parameters than predicted by the sensitivity studies.

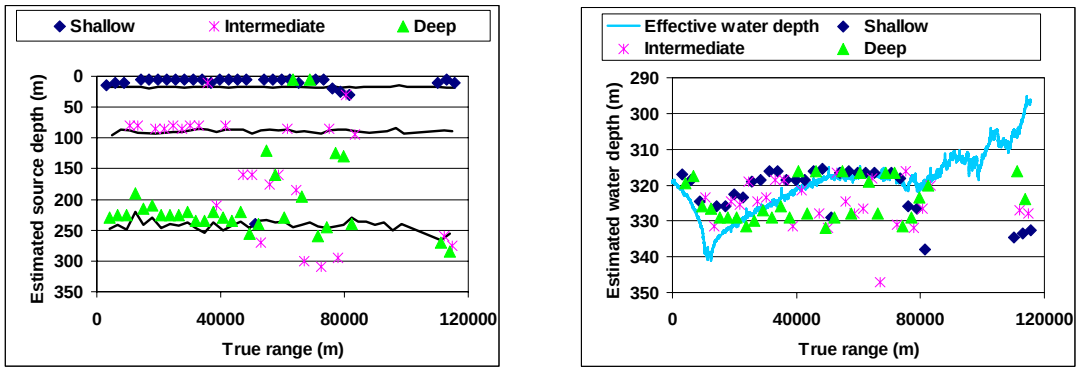

Figure 3.6 *Source depth estimates (left) and water depth estimates (right) for all the shots in the eastern run with Bartlett energy E<0.68. Effective water depth is also plotted.*

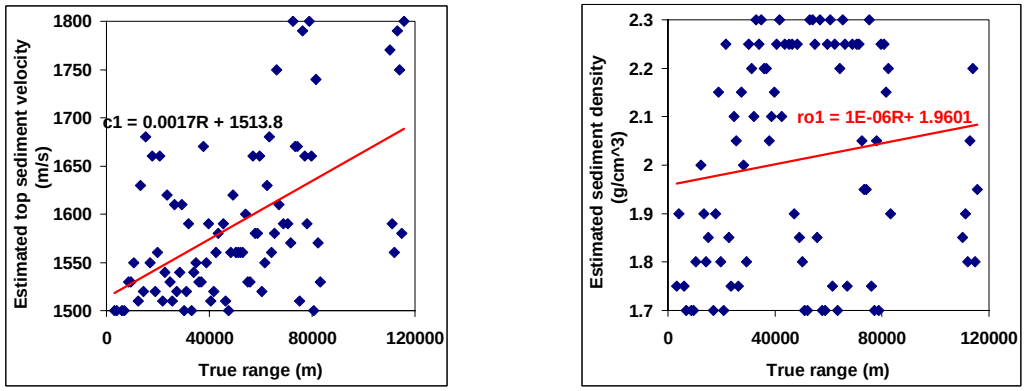

Figure 3.7 *Estimates for top sediment velocity and sediment density for all the shots in the eastern run with Bartlett energy E<0.68.*

3.4 Summary

Range estimates for shots received at a 21-element vertical array and processed at 15 frequencies have been successfully found out to 116 km using matched-field processing techniques. Introducing an energy threshold (i e matching requirement), up to 97% of the shots are within ± 15% of true range for the eastern run. For the southern run similar results are obtained, but for the western run the results are not so good, probably due to lower signal-to-noise ratio and more complex geoacoustic environments. Source depth estimates for shots with nominal detonation depth 18 m are successful at all ranges. However, for the 91 m and 244 m sources, the depth estimates degrade beyond 40-50 km for the eastern run and beyond 20-30 km for the western and southern runs. Inversion for the sediment velocity estimates the value to be about 1600 m/s at short ranges. At long ranges higher values give better match between the measured and replica fields.

4 MATCHED-FIELD PROCESSING WITH A HORIZONTAL ARRAY

by Dag Tollefsen

4.1 Background

Matched-field processing (MFP) techniques for underwater acoustics have been applied to localization of acoustic sources in range and depth using vertical arrays (4), while applications to horizontal arrays (3)(20) are less numerous. The present experiment made use of an acoustic array combining these two configurations. This study presents results from matched-field inversion and source localization using data from the horizontal part of the array.

4.2 Methods

The acoustic field measured by an array is correlated with replica fields generated for trial source positions in a model environment. Correlation is here measured using the incoherent broadband Bartlett processor

$$B(r,z) = \frac{1}{M}\sum_{k=1}^{M} \mathbf{q}^{+}(r,z,\omega_k;\mathrm{m})\mathbf{R}(\omega_k)\mathbf{q}(r,z,\omega_k;\mathrm{m}) \tag{4.1}$$

with **q** the synthetic acoustic field for trial source range r and depth z, $\mathbf{R}=\mathbf{pp}^{+}$ the data covariance matrix constructed from the measured acoustic pressure field **p**, all terms at frequency ω_k and normalized to unity. The model parameters used in computation of replica fields are collectively denoted m. To stabilize results, an incoherent average of M frequencies is formed (21). MFP as applied here requires the acoustic field to be measured over an array of some aperture, but requires no a priori knowledge of the source spectrum or levels. This suits the application to explosive sources.

A two-step approach is adopted. In the first step, model environment parameters are estimated by matched-field inversion of data from a few known sources. In this step, source positions are known and a set of geoacoustic model parameters is searched for in an iterative optimization process. In the second step, the model environment is fixed, and the position of a source is searched for. In this step, an exhaustive search over a large range-depth grid is performed.

4.3 Geoacoustic Inversion

Multi-frequency data (five frequency components within 40-120 Hz) was taken from from six short-range shots (ranges 3-9 km) in two directions endfire to the horizontal array. A two-layer range-independent seabed model consistent with geophysical data was used. The model was described by seven geoacoustic parameters. The search for an optimal set of model parameters (a model that minimizes the cost function E=1-B) was done using an implementation of the adaptive simplex simulated annealing (ASSA) search method (22).

Inversions of data from the ten-element HLA were compared with inversions using data from the 21-element VLA. Figure 4.1 shows results obtained for estimates of two parameters, the sediment and substrate p-wave velocities.

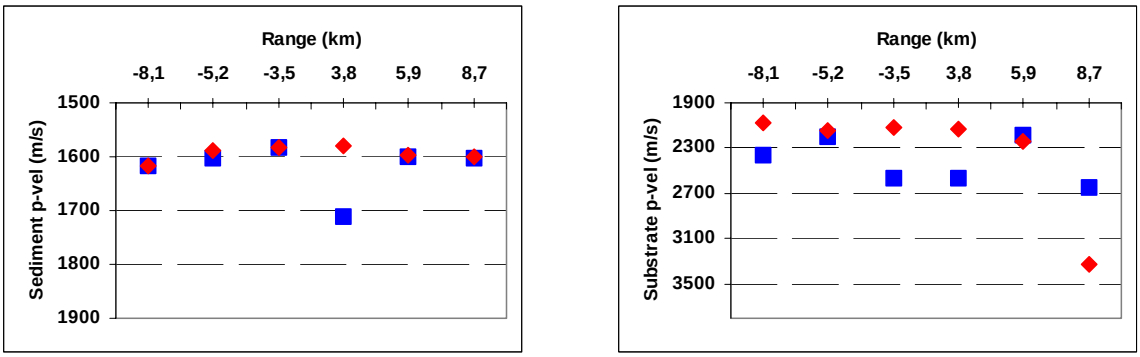

Figure 4.1 *Seabed geoacoustic model parameter estimates obtained by matched-field inversion of multi-frequency shot data from six sources at range 3-9 km on the VLA (red markers) and the HLA (blue markers).*

These results were reported in (23) and more extensively in (24). The use of a HLA for geoacoustic inversion can be of interest in practical respects where deployment of a VLA is not feasible or desirable.

4.4 Source Localization

Shots at nominal ranges 1-60 km (true ranges determined from GPS positions) and nominal depths 18 m and 90 m (true depths determined by analysis of measured bubble pulse periods) from the eastern run were considered in this study. For each shot, a 16k FFT was applied to unfiltered time segments of length 6.5 seconds.

The model environment consisted of a measured sound speed profile in water and a two-layer seabed model. The seabed model parameters are listed in Table 4.1.

Layer	Thickness [m]	P- velocity [m/s]	P-attenuation [dB/λ]	Density [g/cm^3]
Sediment	*30.0*	*1590*	*0.20*	*1.80*
Substrate		*2200*	0.10	2.20

Table 4.1 *Seabed geoacoustic model. Parameters in italics were obtained by matched-field inversion of HLA data from sources at ranges from 3 km to 9 km. Additional seabed parameters are from the baseline geophysical model.*

To account for moderate range dependence in bathymetry, the water depth for an equivalent flat bathymetry was computed from an integral over the measured bathymetry profile (25). This was done for each grid range of the ambiguity surface. Replica fields could then be computed in a fast manner using the normal mode propagation code C-SNAP (18) in range-independent mode. The computation of each ambiguity surface took less than one minute on a 1 GHz Pentium processor.

MFP was tested using data from (i) five frequency components within 40-120 Hz, (ii) one or two 6 Hz wide frequency band centered between 38 Hz - 94 Hz, in this case averaging over ten to twenty frequency components and (iii) sixty frequency components within 38 - 94 Hz. Results are here shown for case (ii) only.

Ambiguity surfaces for two selected shots are shown in Figure 4.2. A color scale set relative to the main peak (red) with a lower threshold of one-half of the peak (-3 dB) (dark blue) is used. The left panel shows results for a deep shot at range 8 km, the right panel for a shallow shot at range 20 km. Both sources were successfully localized in range and depth.

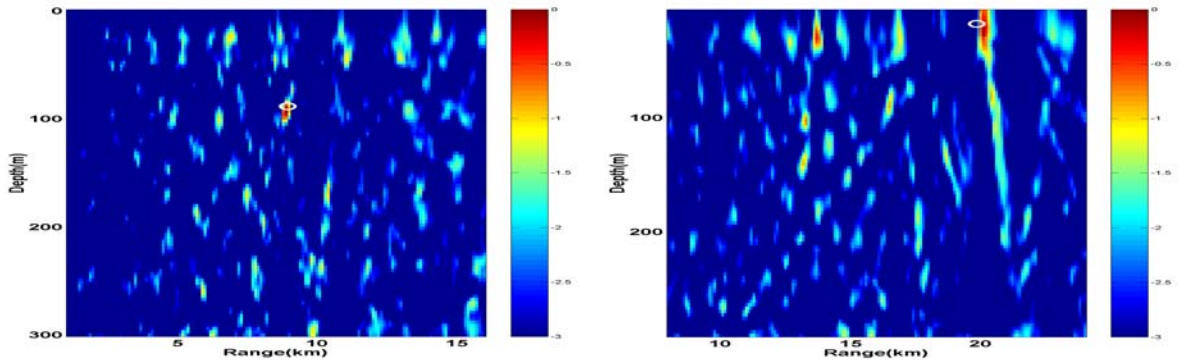

Figure 4.2 *Ambiguity surfaces obtained using the incoherent broadband Bartlett processor applied to data from two 6 Hz wide frequency bands centred at 40 Hz and 90 Hz. Shot data recorded endfire to a ten-element horizontal array at the seabed. A white circle indicates the nominal source range and depth.*

Range and depth estimates for shots at range 1-60 km using data from a 6 Hz wide band centered at 40 Hz are shown in Figure 4.3. For ranges 1-48 km, all but two shots were localized to within 2 km in range and 12 m in depth. At longer range, depth estimates of deep shots degraded. It is assumed that this is a propagation effect: at long range, higher-order steep-angle modes are attenuated to an extent such that sufficient information for depth estimation is not available in the measured acoustic field.

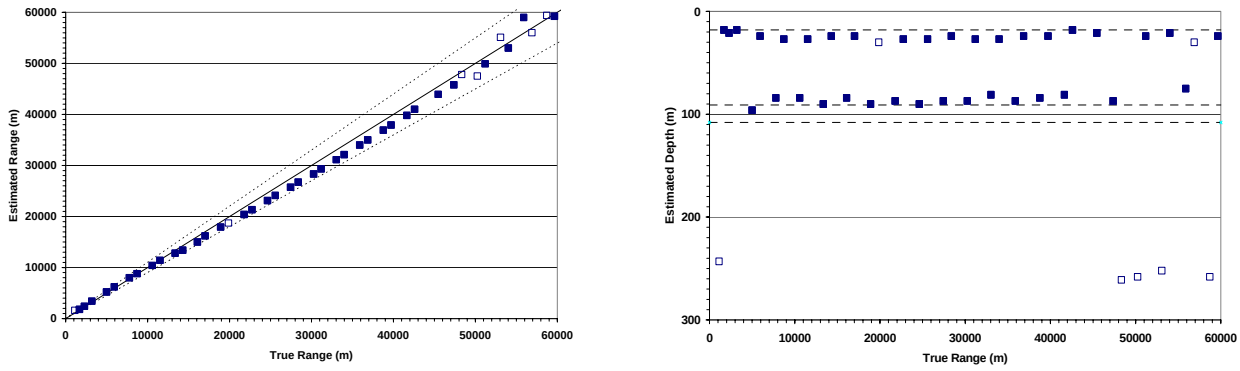

Figure 4.3 *Range (left panel) and depth (right panel) estimates by MFP of shot data recorded endfire to a ten-element bottom-laid horizontal array of length 820 m. Data from a 6 Hz wide frequency band centred at 40 Hz. Filled symbols indicate estimates within 10 % in range and 12 m in depth of nominal.*

Using data in alternative frequency bands within 38 Hz - 94 Hz, results were in general inferior to those presented here (26)(27). This can be understood as a limitation imposed by the present array: for frequencies above ~55 Hz the number of modes in the acoustic field exceeds the number of array elements, and degraded performance can be expected (28). Data was also processed using sub-arrays of shorter length and less number of elements. For example, using data at 40 Hz and a seven-element array of length 740 m, results were comparable to those presented here (29). The issue of array performance for matched-field processing with horizontal arrays warrants further research.

4.5 Summary

Range and depth localization of broadband explosive sources by matched-field processing of data from a bottom-laid horizontal array has been investigated. The incoherent broadband Bartlett processor was used with low-frequency data within 38-94 Hz. Requirements to environment knowledge were a known bathymetry profile of moderate range dependence and a low mismatch seabed model. It was shown that estimates of seabed geoacoustic model parameters could be obtained by matched-field inversion of data from the bottom laid array. The methods should be applicable in shallow water environments similar to the one investigated here. An extension of methods to sources in directions other than endfire to the array should be possible, as long as there is a minimum horizontal aperture of the array.

5 ACOUSTIC DESCRIPTION OF THE EXPERIMENTAL AREA

by Knut A Søstrand

5.1 The experimental area as acoustic waveguide

An underwater acoustic waveguide is characterized by *normal modes*. A mode can be thought of as a signal path that bounces between surface and bottom with a *preferred* up-and-down propagation angle. The number of preferred angles is limited, and determined by phase interferences. By long-range propagation, modes with steep propagation angles produce many surface and bottom reflections incurring losses, and become dampened, reducing the number of effective modes. The number of modes and preferred angles are highly frequency dependent.

A waveguide can be varying with range, for instance if the water depth is not constant. The normal modes still exist. If there is no energy exchange between modes caused by this variability, the waveguide is said to be *adiabatic*. The present experimental area appears to be such a range variable, but adiabatic waveguide. Considering both the shallowness of the sea, the ranges involved and the low noise, the area seems well suited for acoustic waveguide studies.

The sea bottom in the area has a relatively thin sediment layer on top of the substrate or bedrock. For very low frequencies, well below 50 Hz, say, the top of bedrock acts as the apparent bottom, the sediment layer becoming more or less transparent. More about this in Chapter 7.

Perhaps the best way to demonstrate the concept of the area as an acoustic waveguide, is to show the received signal from a SUS detonation, Figure 5.1. This is a sort of LOFAR diagram for the signal, with a vertical time axis and a horizontal frequency axis. The frequency axis is logarithmic in this case, which is a convenience but not a necessity. Take any frequency, the received signal will be a series of pulses. Each pulse represents a normal mode, with its propagation path and propagation time. The steeper the mode angle is, the longer is the propagation time. Following a mode over many frequencies, a continuous pattern can be seen. Each mode has a distinct propagation time maximum or *group speed* minimum. This is called *Airy phase*.

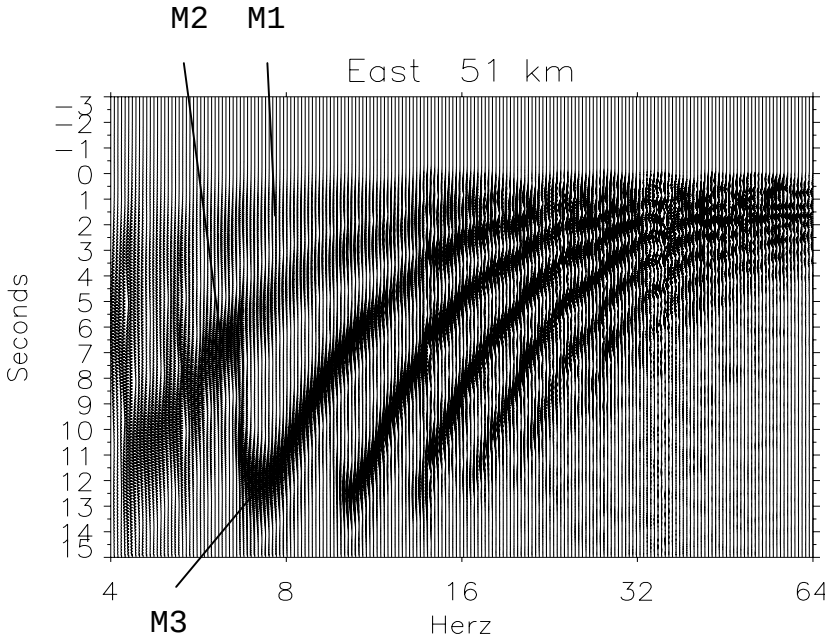

Figure 5.1 Spectrogram for a shot from 51 km east. Hydrophone is at the sea bottom.

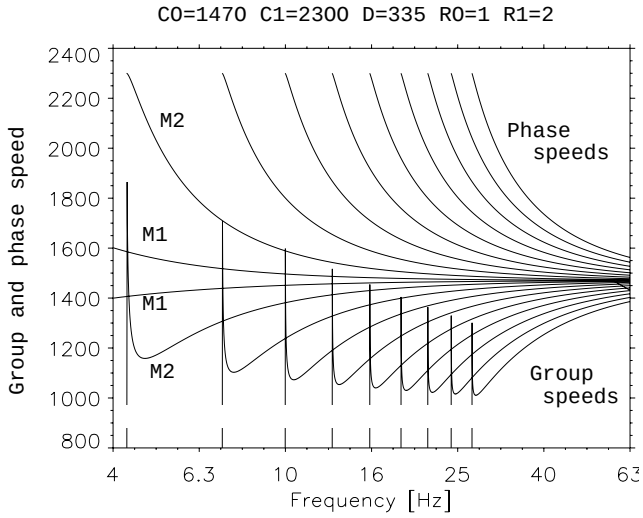

Figure 5.2 A Pekeris analogue.

Figure 5.2 shows theoretical signal speed curves for a so-called Pekeris waveguide (constant-speed water over a constant-speed, constant-depth semi-infinite bottom). The resemblance of the lower set of curves (group speeds) with Figure 5.1 is evident.

Figure 5.3 is another way of presenting data. It shows a narrowband-filtered part of a shot signal as received on the different hydrophones in the vertical part of the array. As before, the lower order modes arrive first. Following a mode from the top downwards, it will go through a series of nulls, the number of nulls increasing with mode number. This change of mode amplitude with depth can be described by the so-called mode functions or eigenfunctions of

waveguide theory. All together, this strongly suggests that the experimental area can be modelled in terms of waveguide theory. This has many advantages, as waveguide computer models in general are simple and fast. More examples of data diagrams can be found in (30).

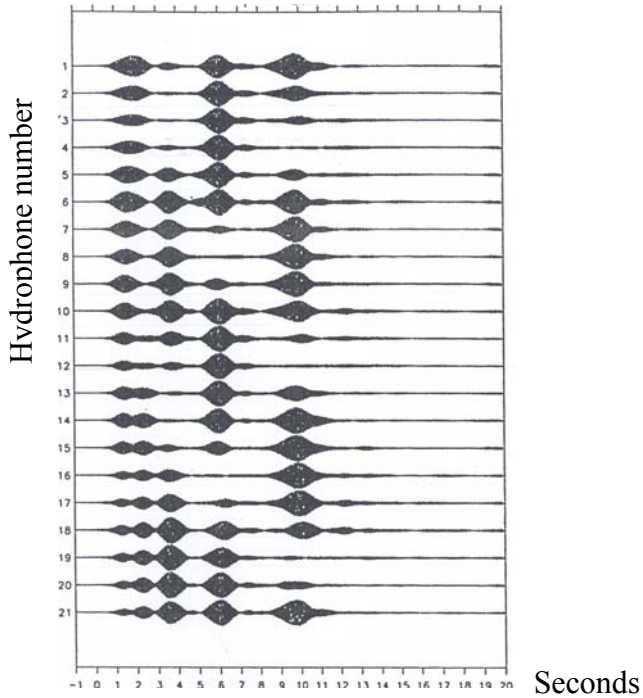

Figure 5.3 Hydrophone signals versus time at 16 Hz.

5.2 Transmission loss and spatial coherence

There are some traditional quantities that can be extracted from an experiment like this, for instance *transmission loss* and *spatial coherence*. Both can be used in the sonar equation. At the present time these quantities have been computed, but not reported formally yet (31). Transmission loss will be given in terms of 9 diagrams (3 runs, 3 source depths). They show the typical shallow-water characteristic of high losses towards both low and high frequencies.

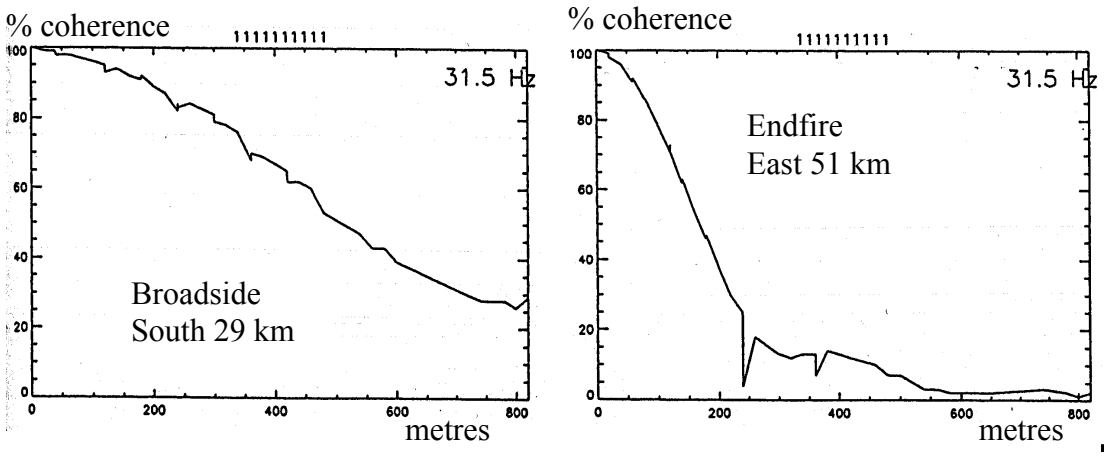

Figure 5.4 Spatial coherence loss, broadside and endfire at 31.5 Hz.

Figure 5.4 gives spatial coherence losses in a 1/3-octave band around 31.5 Hz for a broadside shot and for an endfire shot, respectively. As coherence loss reflects the angular spread of the incoming signal, the endfire case has the higher loss, because of the vertical angular spread of the modes. A broadside array can not resolve vertical angles, it can show only horizontal angular spread, which is much smaller than the vertical. The case here gives for broadside a 50% coherence length of about 500 m, or 10 wavelengths. For endfire it gives 170 m, or 3.5 wavelengths. More coherence examples are given in (31).

This demonstrates a problem with plane-wave beamforming: reduced bearing resolution near endfire. Model-based methods can be able to resolve and recombine multipaths or modes, and give better bearing resolution and better signal to noise ratio. In other words, such methods will better be able to exploit the potential of hydrophone arrays than plane-wave beamformers. The matched-field methods described in this report are further steps in that direction.

6 RANGE LOCALIZATION BY THE β METHOD

by Knut A Søstrand

The β method is a kind of direct way to range localization which can work in range variable, but relatively smooth waveguides. It is different from matched-field localization and does not need model computations. It goes directly upon measureable time and phase differences between mode signals in order to produce the range estimate.

In waveguide theory there has been defined certain quantities that are constant for a given waveguide, with respect to parameters such as frequency and mode numbering (32)(33). One such *waveguide invariant* is named β and defined

$$\beta(R) = - \frac{1/v_m - 1/v_n}{1/u_m - 1/u_n} = constant \qquad (6.1)$$

where v_m, v_n are phase speeds and u_m, u_n are group speeds for modes m and n, respectively, at the given frequency. Phase speed is the horizontal speed of a signal zero crossing. Group speed is the horizontal speed of a pulse (mode) envelope. These speeds are different, usually the phase speeds are higher than group speeds and the speed of sound (Figure 5.2). Group speed is usually lower than the speed of sound. The β of Equation 6.1 is constant over frequency and m and n, but changing with range R when the waveguide is range variable. In order to find β, the speeds must be inferred from the data.

Application of the β method is treated in (34)(35)(36). The receiver configuration uses a horizontal endfire array for resolving normal modes in vertical angle. It uses a filterbank or frequency analyzer for resolving modes in frequency and time. Modes which propagate near horizontally, with grazing angles well away from the critical angle, are selected. Then the reflections from surface and bottom are near perfect (except for phase shift). The endfire array makes it possible to isolate those modes.

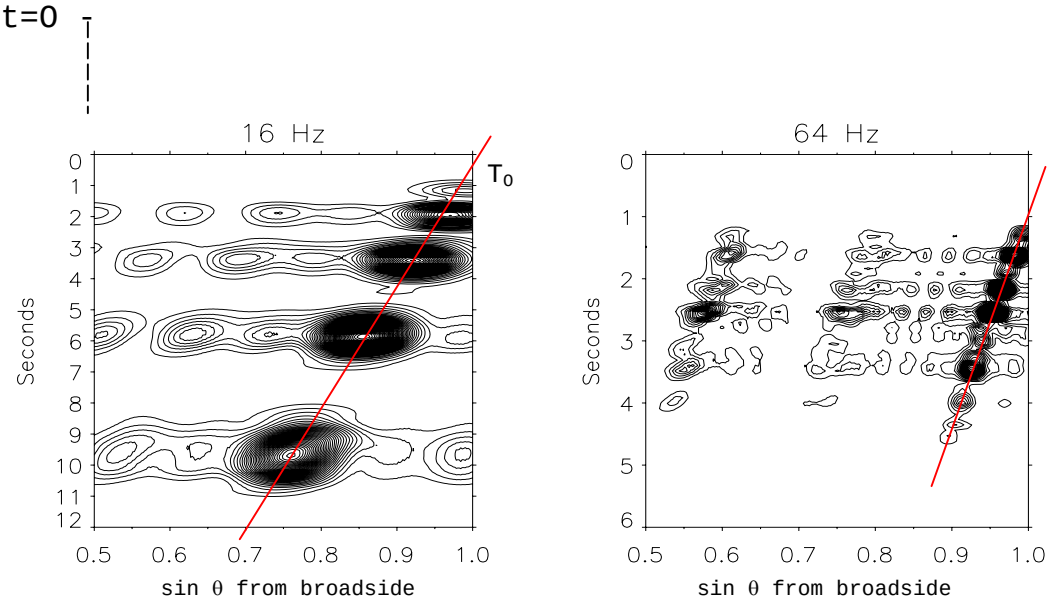

Figure 6.1 *Beam-time diagrams for the eastern 51 km shot at two frequencies. Time scale is relative. Filter bandwidths = 1/12 octave.*

The key step in the signal processing is to compute *beam-time* diagrams, Figure 6.1. The broadband shot signal has now been split into narrow bands, of which two are shown here. The diagrams show how the shot signal (the mode pulses) arrives in time and vertical direction, the direction given as sine to the incidence angle. It turns out that mode arrivals for not-too-large grazing angles lie on straight lines. The *slope* of such a line can be read off the diagram. The slope is steeper the longer the range between source and receiver is (more time spread between the modes). *This is the main clue for range estimation*. In a constant (flat) waveguide there would be a direct proportionality between slope and range, which can be shown to be (34)

$$R = -\beta \, c_0 \, slope \tag{6.2}$$

where c_o is speed of sound in water and the slope is negative. When the waveguide becomes range variable, this relationship is not linear. β becomes a function of range, such that

$$R = -\beta(R) \, c_0 \, slope \tag{6.3}$$

In a Pekeris waveguide the invariant β is simply β = 1. The β factor for range variable waveguides can be developed starting from Equation (6.1) and using the bottom profile, resulting in the formula (33)

$$\frac{1}{\beta(R)} \approx d^2(0) \frac{1}{R} \int_0^R \frac{dx}{d^2(x)} \tag{6.4}$$

where

d(0) = the sea depth at the receiver
d(x) = the bottom profile

Equation (6.3) is easily solved for R.

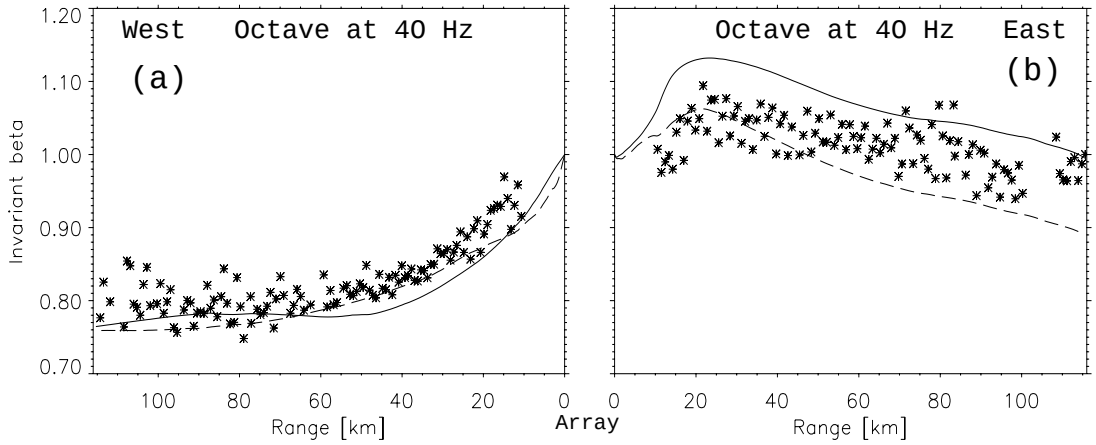

Figure 6.2 Comparisons of theoretical and measured β values. Solid lines = β ref sea bottom. Broken lines = β ref top of bedrock. Asterisk = measured β.

Figure 6.2 shows β values at 40 Hz for the western and eastern endfire runs, respectively, with

- continuous line = β values from Equation (6.4) using the sea bottom
- broken line = β values from Equation (6.4) using the top of bedrock
- asterisks = β values as measured from data diagrams (a cross for each shot).

The measured data are computed from a combination of narrowband slopes (Figure 6.1) within an octave band around 40 Hz. In the western run the β difference between sea bottom and top bedrock is small, in the eastern run it is more substantial. But at this low frequency the measured values confirm best with the top bedrock.

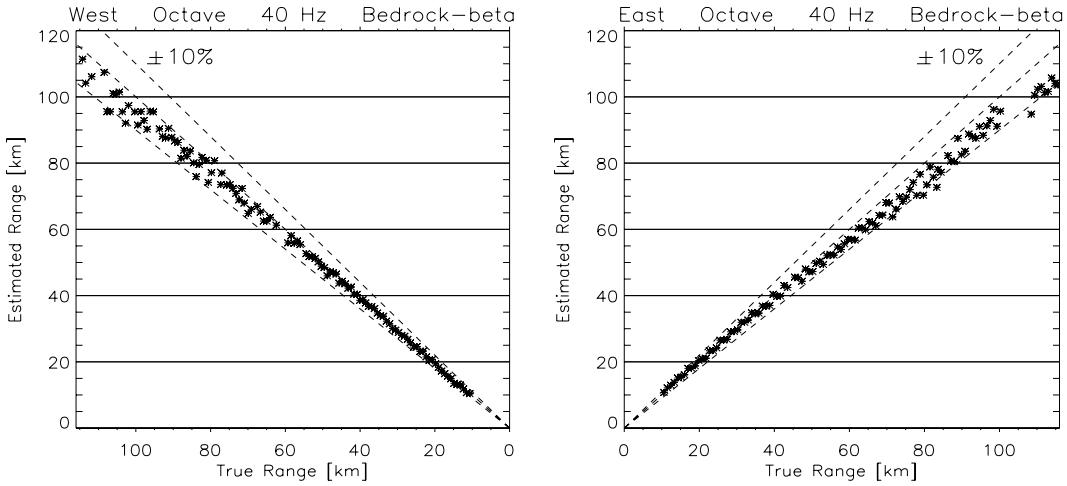

Figure 6.3 Range estimates at 40 Hz.

Figure 6.3 shows range estimates according to Equation (6.3) using data from an octave around 40 Hz, for the western and eastern run, respectively. Typically, the estimates have accuracies of ±5 - ±10%.

Similar accuracies can be expected in areas with fairly gentle range variability, such as here. The acoustic "contrast" i e speed difference between water and bottom/bedrock should be relatively large, such that the critical angle becomes large, and several modes with near-ideal reflections are trapped in the waveguide. Use of the β method is described extensively in (34), together with range estimate diagrams for different frequencies and bandwidths.

7 SINGLE HYDROPHONE LOCALIZATION OF SHOTS

by Trond Jenserud

7.1 Introduction

In this section the problem of localizing a shot signal from measurements on a single hydrophone (37) (38) (39) will be considered. More specific, we are aiming for methods suitable for localizing broadband explosive sources at long ranges (30-100km) in a shallow water environment (40). The primary objective is estimation of range, but the feasibility of determining source depth and direction of source from a single hydrophone measurement will also be considered.

7.2 Methods

The main difficulty associated with single-hydrophone localization is the lack of spatial information. Conventional MFP depends on the spatial structure of the sound field to localize a source. In the case of a single hydrophone the lack of spatial information must be compensated by utilizing temporal information.

It is convenient to classify the methods for single-hydrophone localization into two categories depending on the source type: the source waveform may be either known or unknown. In the first case range can be estimated by waveform inversion, in the second case range can be estimated using the dispersive properties of the waveguide.

7.2.1 Known source waveform

Several non-deterministic source types produce signals that are so repeatable that a signal model can be used to represent the source. Among such sources are SUS charges. The signal generated by an explosive charge depends on detonation depth and charge weight, and the signal model therefore contains these quantities as parameters. A method for localizing an explosive source is to use a proper signal model and include the source waveform parameters in the parameter vector for inversion.

7.2.2 Unknown source waveform

When the source waveform is unknown we have to rely on methods that utilize waveguide properties only. Figure 7.1 shows signal dispersion in a shallow water waveguide of the Pekeris type (a homogeneous water layer overlaying a homogeneous fluid halfspace). A waveguide of this type supports modal propagation, and the modes are dispersive, i e, the group velocity varies with frequency. As a consequence of dispersion, the signal is gradually stretched as it propagates outwards. At a range of 30 km the total signal dispersion is 0.7 s, and the three wavepackets seen are actually mode 1, 2 and 3. Knowing the waveguide

parameters, range can be estimated either from the total dispersion of the pulse, or from the time differences of modal arrivals. The latter is the preferred method.

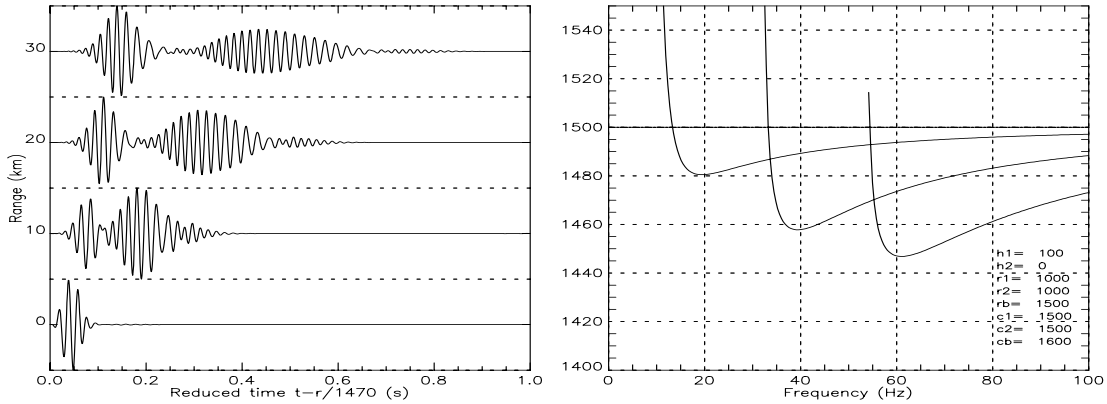

Figure 7.1 Signal dispersion in a Pekeris waveguide demonstrated by pulse simulations at 0-30km (left panel) and group velocity for the three first modes (right panel). The source has a bandwidth of 50 Hz and is centred around 50 Hz.

7.3 Range estimation by time differences of modal arrivals

As shown above, source range can be estimated from the dispersion characteristics of a waveguide. By measuring the travel time differences of a pair of modes, Δt_{nm}, the range is found by

$$R = \frac{\Delta t_{nm}}{1/u_n - 1/u_m} \tag{7.1}$$

where u_m and u_n are the group velocities of mode m and n respectively. The method requires that the modal arrivals can be separated at the receiver, in the receiver bandwidth. The method will therefore not work at close ranges.

Modal arrival times can be extracted from frequency-time (FT) plots of the data. Figure 7.2 (left panel) shows a FT-plot of a shot at 59 km range. The modal arrivals are clearly separated at low frequencies. At 10 Hz the first arrival is a weakly excited 1st mode followed by more strongly excited modes 2 and 3. Based on travel time differences between modes 2 and 3 an estimated range of 62 km is obtained. The result depends strongly on the choice of geoacoustic model. In this case a Pekeris waveguide with depth 330 m and bottom speed 2200 m/s is assumed. The red curves overlaying the FT-plot are arrival times of the modes, obtained from dispersion curves computed from the Pekeris model.

The Pekeris waveguide is a reasonably accurate model for the waveguide at low frequencies. For frequencies above 20 Hz (for the present environment) there are discrepancies, due to effects of a sediment layer, and a three-layer fluid model with homogeneous layers is a better model. This is demonstrated in Figure 7.2 (right panel), which shows a comparison of

dispersion curves computed for a three-layer model and a Pekeris model for which the parameters have been adjusted to obtain good match with the three-layer model at low frequencies. Such an equivalent Pekeris model is a valid approximation for frequencies below 20 Hz for the present environment. The advantage of the Pekeris model is its computational efficiency. To retain an efficient algorithm in the case of weak range dependence, optimal equivalent bathymetry (25) could be incorporated into the model.

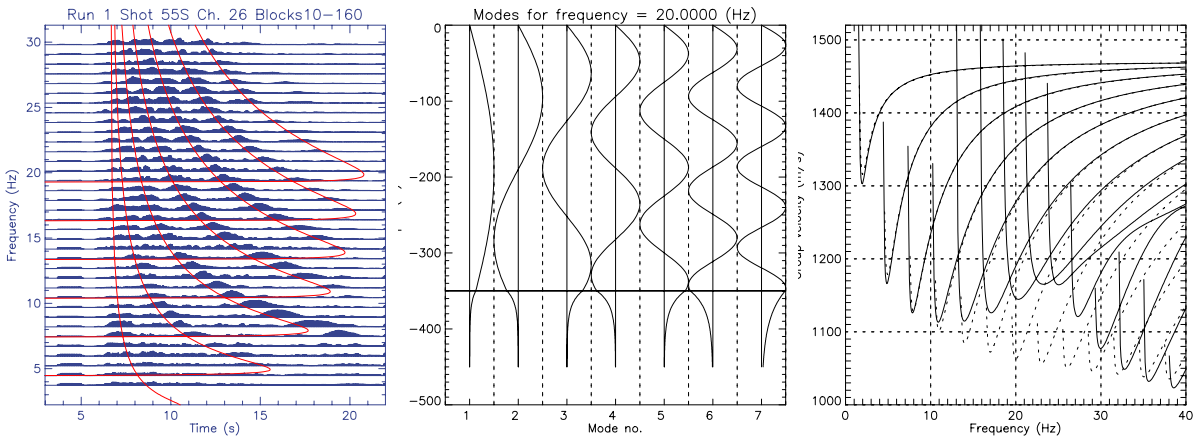

Figure 7.2 *Frequency-time plot of shot (left panel) and mode function for the first 7 modes at 20 Hz (mid panel) and dispersion relations (right panel) for a three-layer model with parameters c_1=1470m/s, ρ_1=1.0, h_1=320m, c_2=1620m/s, ρ_2=1.8, h_2=30m, c3=2250, ρ_3=2.2 (solid line) and an equivalent Pekeris model with c_1=1470m/s, ρ_1=1.0, h_1=330m, c_2=2200m/s, ρ_2=2.2 (dotted line).*

Obtaining accurate source range estimates from time differences of modal arrivals not only requires a good geoacoustic model such that the group velocities are correctly estimated, it also requires a correct identification of the modes. Factors that may cause misinterpretation of modes are noise and weakly excited modes due to the depth and the frequency content of the source. The depth dependence of modes is illustrated in Figure 7.2 mid panel.

An important question is how well it is necessary to know the acoustic environment to obtain reliable estimates of source range. This problem can best be approached by a sensitivity analysis. Figure 7.3 shows the sensitivity of range to mismatch in water depth and bottom sound speed for a Pekeris waveguide, for a source at nominal range 50 km. The most sensitive parameter is the bottom sound speed, followed by water depth. Sensitivity to water sound speed and density contrast is low (40).

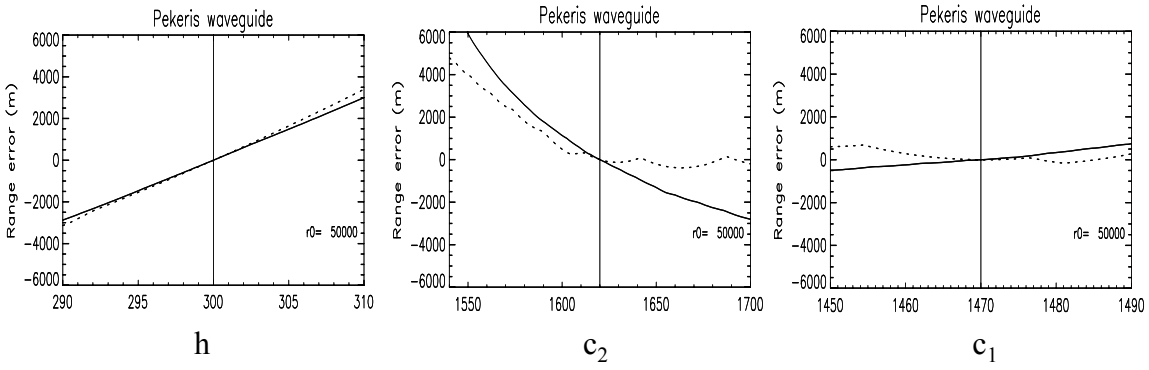

Figure 7.3 Sensitivity of range for mismatch in water depth (left panel), bottom sound speed (mid panel) and water sound speed (right panel) for a Pekeris waveguide for 20 Hz (solid line) and 40 Hz (dotted line). Range is estimated from time difference of modes 2 and 3. Nominal water depth 300 m, bottom sound speed 1620 m/s and water sound speed 1470 m/s.

7.4 Source localization by waveform inversion

If the source waveform can be assumed known, source localization can be performed by waveform inversion: the waveform measured by the hydrophone is compared to synthetic waveforms computed for a number of trial source positions. Other parameters, such as source depth, charge weight and waveguide properties may also be determined by the inversion.

The components of a waveform inversion scheme include a source model, a forward model (acoustic propagation model), a geoacoustic model, an objective function and a global search method. In the present study we have used a Wakeley source model (41), in which the waveform depends on source depth and charge weight, a simple normal mode propagation model, and a Pekeris geoacoustic model. The objective function used here measures the correlation between measured and synthetic FT-plots, and has the form

$$E(r,z) \cong \sum_i \sum_j W(\omega_i, t_j) \, | \, FT(\omega_i, t_j)_{obs} - FT(\omega_i, t_j)_{calc} \, | \tag{7.2}$$

where FT_{obs} and FT_{calc} are normalized observed and calculated frequency-time spectra and W is a weight function. The objective function is a crucial element of the inversion method.

The influence of model parameters on the objective function was investigated by computing the value of the objective function for a number of parameter pairs (ambiguity surfaces). In the computation of the objective function a frequency range of 7-18 Hz was used. Figure 7.4 shows ambiguity surfaces for three parameter combinations for a shot at range 36.8 km.

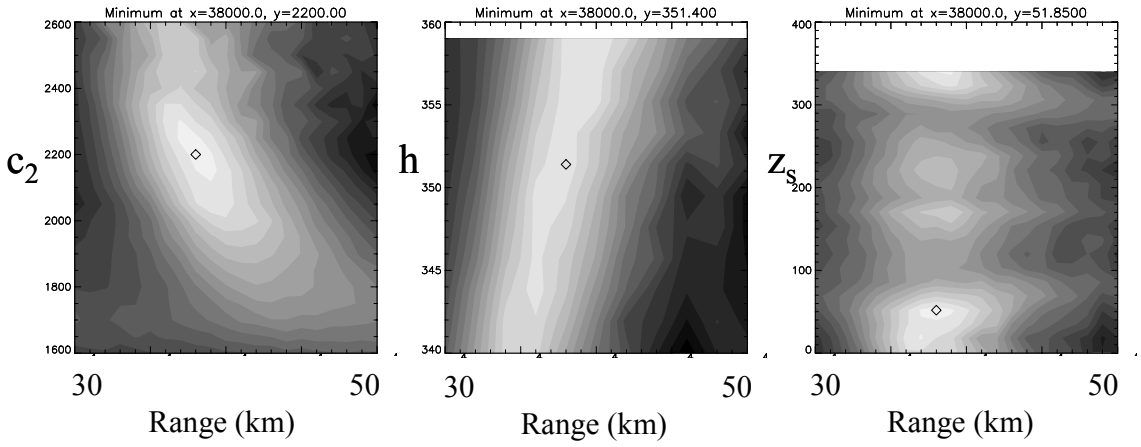

Figure 7.4 Ambiguity surfaces for range and bottom sound speed (left panel), range and water depth (mid panel) and range and source depth (right panel). True range is 36.8 km and true depth is18m.

The plots show that bottom sound speed and water depth are sensitive parameters. Assuming too large value of bottom sound speed causes underprediction of range while too large water depth causes range to be overpredicted. The ambiguity surfaces are smooth, exhibiting relatively low resolution, but also low sidelobes. The method also shows some ability to localize in depth, as shown in the right panel of the figure, although sidelobes are considerable in this case.

The method has been applied to a few shots in the range of 36-86 km. Range predictions for three shots at nominal ranges 36.8, 59.6 and 83.5 km are shown in Figure 7.5. Predicted ranges were 36, 62 and 90 km respectively.

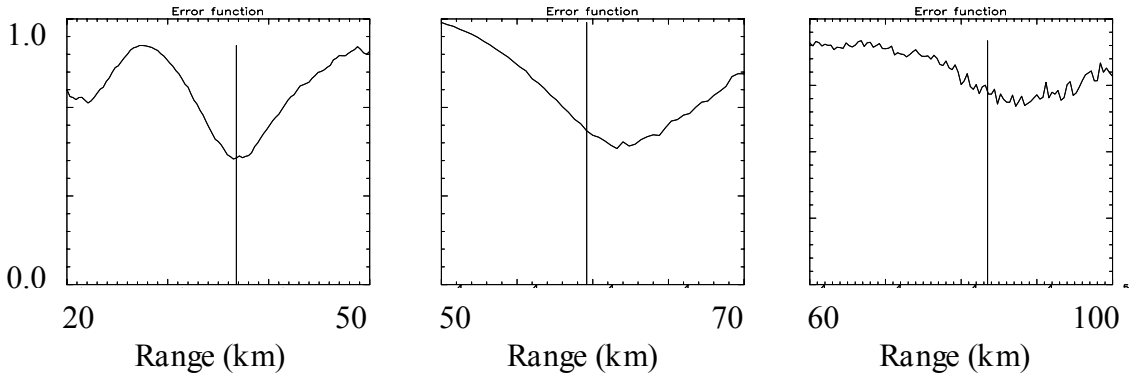

Figure 7.5 Value of objective function for three shots at nominal ranges 36.8, 59.6 and 83.5 km. Source depth is 18 m. The receiver is located on the bottom. Vertical line indicates true range.

7.5 Summary and discussion

Two methods for single-hydrophone localization of shot signals have been studied. The first method estimates range from time differences of modal arrivals, and does not use information about source waveform. The second method assumes a signal model, and estimates source

range and depth by waveform inversion. A crucial element of the inversion method is the objective function.

The methods have been applied to shot data from the SWASI-99 experiment, on a small number of shots. The shots were localized with reasonable accuracy for source ranges of 36-86 km. A certain ability to localize in depth is also demonstrated. Localization in azimuth by a single-hydrophone method is considered not feasible.

In the validation against real data a simple Pekeris waveguide has been used to model propagation. The Pekeris model is shown to be a valid approximation for low frequencies, typically below 20 Hz. At higher frequencies the effect of a sediment layer needs to be accounted for. A three layer fluid model seems adequate for the present geoacoustic environment. For waveform inversion a fast broadband model is required, and the use of an equivalent Pekeris model provides an efficient algorithm.

The methods have been demonstrated for relatively ideal conditions: in an acoustically benign area and with a high signal-to-noise ratio. The performance of the methods in less ideal conditions is difficult to predict in advance, and need to be tested against real data.

Estimation of direction to a source using a single hydrophone is a difficult problem. In theory it can be done if each source point has a unique Greens function with respect to the receiver. Such ‘symmetry breaking’ environments may be found in some places. However, it is unlikely that direction estimation can be achieved in relatively flat areas.

8 SUMMARY

The localization of underwater sources in a shallow water environment has been addressed. Several model-based signal processing methods were applied to low-frequency acoustic data acquired in an experiment conducted in the Barents Sea. The methods are model based in the sense that a model of the waveguide and/or a model of the acoustic propagation is incorporated in the signal analysis or signal processor.

Matched-field methods were applied to vertical array data and to data from sources endfire to a bottom-laid horizontal array. Good range estimates were obtained with data from both array configurations. Depth estimates tended to degrade at long range. Seabed model parameters were estimated by matched-field inversion of data (results shown for both array configurations) or incorporated as optimization parameters in the localization (shown for vertical array data).

The β-method for range estimation uses information on the bathymetry of the waveguide and features characteristic of the waveguide propagation extracted from conventional beamformed horizontal array data. The method produced good range estimates. The azimuth direction (here: endfire) must be known, and an environment of moderate range dependence in bathymetry is assumed.

Source localization using acoustic data from a single hydrophone was investigated using two methods, one using temporal properties of the signals (time difference of modal arrivals), one using a source model and a full-field model of the acoustic propagagation. Promising results were obtained from both methods.

For the relatively flat and homogeneous environment of the present experiment, the methods worked to produce good range estimates and in most cases good depth estimates of near to far-away explosive sources. An extension of the methods to more complicated environments (in bathymetry and seabed composition) and to other sources (time-harmonic signals from moving sources, lower signal levels and sources in non-endfire directions to a horizontal array) is a required next step of investigation.

References

(1) Bucker H P (1986): Use of calculated sound fields and matched-field detection to locate sound sources in shallow water, *J Acoust Soc Am* **59**, 368-373.

(2) Baggeroer A B, Kuperman W A and Mikhalevsky P N (1993): An overview of matched field methods in ocean acoustics, IEEE *J Oceanic Engineering* **18**, 401-424.

(3) Ozard J M (1989): Matched field processing in shallow water for range, depth, and bearing determination: Results of experiment and simulation, *J Acoust Soc Am* **86**, 744-53.

(4) Jesus S M (1993): Broadband matched-field processing of transient signals in shallow water, *J Acoust Soc Am* **93**,1841-1850.

(5) Chapman N R and Taroudakis M (eds.) (2000): Geoacoustic inversion in shallow water, *J Computat Acoustics* **8**, 2.

(6) Johnsen J (1999): SWASI II - Cruise Report, Phase S-V 1999, FFI/NOTAT-99/05715, Forsvarets forskningsinstitutt, Exempt from public disclosure.

(7) Eidem E J, Bendiksen B, Helgesen H (1999): Project Swasi: Technical Cruise Report from Phase S-V 1999, FFI/RAPPORT-99/04955, Forsvarets forskningsinstitutt, Exempt from public disclosure.

(8) Eidem E J (2000): A 1040 m Deployable Hydrophone Array and its Data Acquisition System - Part I: General description and data formats, FFI/RAPPORT-2000/04033, Forsvarets forskningsinstitutt, Exempt from public disclosure.

(9) Eidem E J (2000): A 1040 m Deployable Hydrophone Array and its Data Acquisition System - Part II: Detailed description, FFI/RAPPORT-2000/04034, Forsvarets forskningsinstitutt, Exempt from public disclosure.

(10) Eidem E J (2000): Estimation of the Hydrophone Array Position During Swasi 1999 Phase S-V, FFI/RAPPORT-2000/04107, Forsvarets forskningsinstitutt, Exempt from public disclosure.

(11) Solberg C E (2001):Geoakustiske modeller for MFP eksperiment i Barentshavet august 1999, FFI/RAPPORT-2001/00335, Forsvarets forskningsinstitutt.

(12) Sættem J (1996): Acoustic properties of Quaternary sediments in the southern Barents Sea, *Report no 23.2579.00/01/96*, IKU Petroleumsforskning.

(13) Telford W M , Geldart L P, Sheriff R E (1990): Applied geophysics, Cambridge University Press.

(14) Eidem E J (2001): Single Shot Inversion from the L-Antenna Experiment in 1999, FFI/RAPPORT-2001/02927, Forsvarets forskningsinstitutt.

(15) Eidem E J (2002): Broadband Inversion and Source Localization of Vertical Array Data from the L-antenna Experiment in 1999, FFI/RAPPORT-2002/02565, Forsvarets forskningsinstitutt.

(16) Eidem E J (2003): Localization of Underwater Explosions by Matched Field Processing Techniques – Vertical Array Data from the SWASI-99 Experiment, FFI/RAPPORT-2003/00780, Forsvarets forskningsinstitutt, Exempt from public disclosure.

(17) Gerstoft P (2001): SAGA User Manual 4.1: An inversion software package, SACLANTCEN and Marine Physical Laboratory.

(18) Ferla C M, Porter M B, Jensen F B (1993): C-SNAP: Coupled SACLANTCEN normal mode propagation loss model, SACLANTCEN Memorandum SM-274.

(19) Eidem E J (2003): Localization of Explosions using a Vertical Array, Proceedings of the Tenth International Congress on Sound and Vibration (2003), **5**, 2617-2624.

(20) Schey P W et al (1997): Matched-field processing of multi-tone acoustic signals in shallow water with a horizontal line array, *J Acoust Soc Am* **101**, 3047.

(21) Baggeroer A B, Kuperman W A and Schmidt H (1988): Matched field processing: Source localization in correlated noise as an optimum parameter estimation problem, *J Acoust Soc Am* **83**, 571-587.

(22) Dosso S E, Wilmut M J and Lapinski A-L S (2001): An adaptive-hybrid algorithm for geoacoustic inversion, IEEE *J Oceanic Engineering* **26**, 324-36.

(23) Tollefsen D (2003): Matched-field inversion of horizontal array data from the L-antenna experiment in 1999, FFI/RAPPORT-2003/01003, Forsvarets forskningsinstitutt.

(24) Tollefsen D, Wilmut M J and Chapman N R (2003): Estimates of Geoacoustic Model Parameters from Inversions of Horizontal and Vertical Line Array Data, OCEANS 2003, MTS 0-933957-31-9, 592-597.

(25) Zakarauskas P, Dosso S E and Fawcett J A (1996): Matched-field inversion for source location and optimal equivalent bathymetry, *J Acoust Soc Am* **100**, 1493-1500.

(26) Tollefsen D (2002): Matched-field localization of explosive sources in the Barents Sea using a horizontal array, FFI/RAPPORT-2002/04480, Forsvarets forskningsinstitutt.

(27) Tollefsen D (2003): Range-depth localization of far-away shots by matched-field processing of horizontal array data, FFI/RAPPORT-2003/01767, Forsvarets forskningsinstitutt, Exempt from public disclosure.

(28) Tantum S L and Nolte L W (2000): On array design for matched-field processing, *J Acoust Soc Am* **107**, 2101-2111.

(29) Tollefsen D (2003): Range-depth localization of underwater explosions by matched-field processing of data from a sparse bottom-laid horizontal array, *J Acoust Soc Am* **114**, 2401.

(30) Søstrand K A (2002a): Before inversion of far-away shots, FFI/RAPPORT-2002/00722, Forsvarets forskningsinstitutt, Exempt from public disclosure.

(31) Søstrand K A (200*): Transmission losses. Spatial coherence. FFI/RAPPORT, Forsvarets forskningsinstitutt, In preparation.

(32) Chuprov S D (1982): Interference structure of a sound field in a layered ocean, in Ocean Acoustics, Current State, 1982, edited by L M Brekhovskikh and I B Andreevoi, Nauka, Moscow, pp 71-91, (in Russian).

(33) D'Spain G L and Kuperman W A (1999): Application of waveguide invariants to analysis of spectrograms from shallow water environments that vary in range and azimuth, J Acoust Soc Am **106**, 2454-2468.

(34) Søstrand K A (2002b): Range localization of 10-100 km shots by means of an endfire array and a waveguide invariant, FFI/RAPPORT-2002/04849, Forsvarets forskningsinstitutt.

(35) Søstrand K A (2002c): A minimalistic approach to range localization in a waveguide, 26th Scandinavian Symposium on Physical Acoustics, Ustaoset 26-29 January 2003.

(36) Søstrand K A (2003): Application of waveguide invariants for localization of shots in range dependent waveguides, Proceedings of the 10th International Congress of Sound and Vibration, 7-10 July 2003, Stockholm, Sweden.

(37) Clay C S (1987): Optimum time domain signal transmission and source location in a waveguide, *J Acoust Soc Am* **81**, 660-664.

(38) Frazer L N and Pechols P I (1990): Single-hydrophone localization, *J Acoust Soc Am* **88** (2), 995-1002.

(39) Jesus S M (2000): Single hydrophone source localization, *IEEE J Oceanic Eng* **25** (3), 337-346.

(40) Jenserud T (2003): Single hydrophone localization of shots. Feasibility study., FFI/RAPPORT-2003/01328, Forsvarets forskningsinstitutt.

(41) Wakeley J (1978): Coherent ray tracing – measured and predicted shallow water frequency spectrum, *J Acoust Soc Am* **63**(6), 1820-1823.